Steps in gas-surface reactions

Lent, R. van

Chapter 7

Outlook – CO_2 spectroscopy and state-preparation for state-resolved dissociation experiments

During this PhD work, we started a new project to study state-resolved CO_2 dissociation. To this end, an optical setup was developed to vibrationally excitate CO_2 in the supersonic molecular beam. This line of research will be continued within our research group. As an outlook, we provide a basic description of CO_2 spectroscopy and subsequently explain how we prepare CO_2 in an excited state in the beam.

CO_2 spectroscopy

Spectroscopic observations and interpretation thereof using quantum mechanics has been essential in much of our current understanding of molecules and their structure and energy levels. Here, we present a short introduction into the spectroscopy of CO_2 to provide a foundation for later work. The first half of this chapter is a summary of sections concerning linear molecules from Molecular Spectra and Molecular Structure: II Infrared and Raman Spectra of Polyatomic Molecules by Gerhard Herzberg.[134]

Electromagnetic radiation (photons) can be absorbed or emitted by molecules. The energies of these photons take discrete values that match energy level differences between the initial and final state. On photon absorption, molecules are electronically, vibrationally, and/or rotationally excited. The goal of the experiment is activation of CO_2 by absorption of mid-infrared radiation and subsequent reaction. After excitation, CO_2 will be impinged on a Ni(1 1 7) catalytic surface for state-resolved dissociation, but this is unfortunately beyond the scope of this thesis. Thorough understanding of the experimental results will necessitate a basic understanding of CO_2 spectroscopy, which we provide here. We focus on spectroscopic concepts relevant for the results in this thesis: rotations, vibrations, and combination thereof; so-called rovibrations. Excitation follows selection rules that are governed by symmetry considerations. Therefore, we first delve into the symmetry of linear molecules. Rotations, vibrations, rovibrations are subsequently described. Finally, deviations from these model descriptions are also discussed.

Symmetry

The symmetry of molecules is described by group theory. In group theory, two point groups describe the possible types of linear molecules: $D_{\infty h}$ and $C_{\infty v}$. Molecules with a center of inversion belong to the first, e.g. $C^{16}O_2$, whereas molecules without a center of inversion belong to the second, e.g. OCS or $C^{16}O^{18}O$. In other words, molecules described by $D_{\infty h}$ have no permanent dipole moment, while those with $C_{\infty v}$ do. The spectroscopy for

these two types of linear molecules is different. Symmetry governs whether transitions are infrared and/or Raman active and which rotational states are allowed. From now on, CO_2 refers to the most common isotope, $C^{16}O_2$, unless specified otherwise.

Character tables are used to describe how symmetry species of a point group change upon symmetry operations. Different characteristics of molecules may be of the same symmetry species. The character table for CO_2, $D_{\infty h}$, is shown in table 7.1. Here, the z-axis is defined as the intermolecular axis. Ground state CO_2 has Σ_g^+ character, i.e. it is symmetric (+1) to all symmetry operations.

CO_2 has 3N=9 degrees of freedom: 3 translations, 2 rotations, and 4 vibrations. T_x, T_y, and T_z are translations in the x, y, and z directions. R_x, R_y, and R_z are rotations around the x, y, and z axes respectively. Translation, rotation or vibrational excitation may alter the molecular symmetry so that it is anti-symmetric (-1) to some symmetry operations. ν_1, ν_2, and ν_3 are the three normal modes with Σ_g^+, Π_u, and Σ_u^+ character. The $2\nu_2$ overtone is added to the character table due to the Fermi resonance discussed below.

Table 7.1: $D_{\infty h}$ character table

$D_{\infty h}$	I	$2C_\infty^\phi$	$2C_\infty^{2\phi}$	...	σ_h	∞C_2	$\infty\sigma_v$	$2S_\infty^\phi$	$2S_\infty^{2\phi}$	...	$S_2 \equiv i$	
Σ_g^+	+1	+1	+1	...	+1	+1	+1	+1	+1	...	+1	ν_1, $2\nu_2$ $\ell = 0$
Σ_u^+	+1	+1	+1	...	-1	-1	+1	-1	-1	...	-1	T_z, ν_3
Σ_g^-	+1	+1	+1	...	+1	-1	-1	+1	+1	...	+1	R_z
Σ_u^-	+1	+1	+1	...	-1	+1	-1	-1	-1	...	-1	
Π_g	+2	2cosϕ	2cos2ϕ	...	-2	0	0	-2cosϕ	-2cos2ϕ	...	+2	R_x, R_y
Π_u	+2	2cosϕ	2cos2ϕ	...	+2	0	0	+2cosϕ	+2cos2ϕ	...	-2	T_x, T_y, ν_2
Δ_g	+2	2cos2ϕ	2cos4ϕ	...	+2	0	0	+2cos2ϕ	+2cos4ϕ	...	+2	$2\nu_2$ $\ell = 2$
Δ_u	+2	2cos2ϕ	2cos4ϕ	...	-2	0	0	-2cos2ϕ	-2cos4ϕ	...	-2	
Φ_g	+2	2cos3ϕ	2cos6ϕ	...	-2	0	0	-2cos3ϕ	-2cos4ϕ	...	+2	
Φ_u	+2	2cos3ϕ	2cos6ϕ	...	+2	0	0	+2cos3ϕ	+2cos4ϕ	...	-2	
...	...	...	...	...	...	...	...	...	...	...	...	

Rotations

Rotation of linear molecules in the electronic ground state is well-described by the rigid rotor model. In this model, bond angles and lengths are fixed. Rotational energy levels are approximated using:

$$E_{\text{rot}} = B \cdot J(J+1) \tag{7.1}$$

where B and J are the rotational constant and total angular momentum quantum number (or rotational quantum number).

We exclude a minor correction to account for centrifugal distortions with increasing rotational states. We require quantum mechanics to describe the allowed total angular momentum. The total eigenfunction of a molecule is the product of the electronic, vibrational, and rotational wavefunctions:

$$\Psi = \Psi_{\text{nucl}}\Psi_{\text{elec}}\Psi_{\text{vib}}\Psi_{\text{rot}} \tag{7.2}$$

The wavefunctions for the rigid rotor, Ψ_{rot} can be approximated by spherical harmonics[135] (also called the particle on a sphere), which closely resemble electronic wavefunctions of ^{1}H. For any molecule, the total angular momentum is comprised of the vibrational angular momentum quantum number ℓ, magnetic quantum number M, and spin quantum number M_s (if $M_s = \frac{1}{2}$). CO_2 does not have nuclei with nuclear spin, thereby excluding any hyperfine splitting by M_s. J then only has a 2J+1 degeneracy where M can be -J, -J+1 ... J-1, J. The degenerate wavefunctions for J = 0 to J = 3 are shown in figure 7.1.

Rotations have Π_g character. Note center of inversion operation i for Π_g; the sign of the wavefunction cannot change upon inversion. Examination of the rotational wavefunctions in figure 7.1 shows that the even rotational states, J = 0 and J = 2, are symmetric to the inversion operation. In contrast, all odd rotational states are antisymmetric to inversion. As a consequence, all odd rotational states are missing in the vibrational ground state for molecules with point group $D_{\infty h}$. Odd rotational levels do exist

for excited states containing odd quanta of asymmetric stretch or quanta of bend vibration.

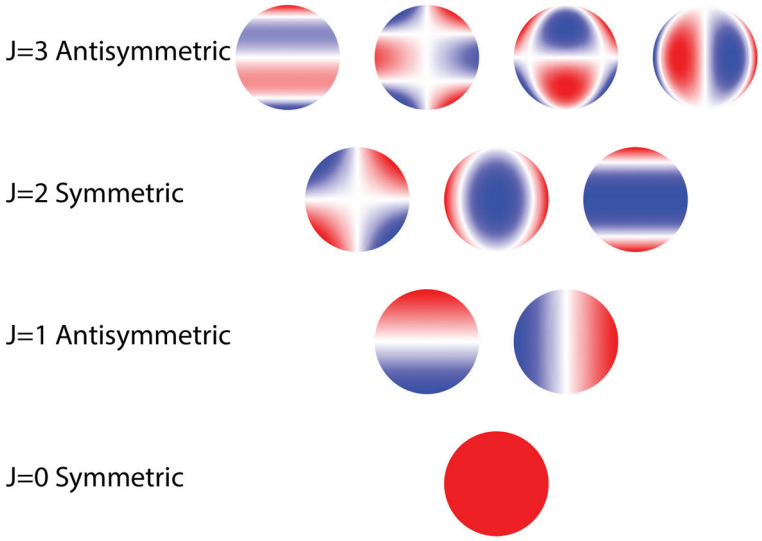

Figure 7.1: Spherical harmonics for J = 0 to 3 with degeneracies M = 0 to +J shown from left to right. Even (odd) J states are (anti)symmetric to the inversion operation.

Generally, pure rotational Raman transitions occur if there is a change in polarizability, while pure rotational infrared transitions are only observed if the molecule has a permanent dipole moment. Pure rotational transitions have the following general selection rules:

$$\begin{aligned} \Delta J_{\text{infrared}} &= \pm 1 \\ \Delta J_{\text{Raman}} &= \pm 2 \end{aligned} \tag{7.3}$$

where J has an integer number of $h/2\pi$. As such, molecules of the $D_{\infty h}$ point group only show a pure rotational Raman spectrum. The previously discussed symmetry considerations prohibit odd rotational states in the vibrational ground state. As for H_2 and D_2, conversion of the symmetric (even) to antisymmetric (odd) rotational levels (or vice versa) is forbidden. A pure infrared rotational spectrum is only observed for CO_2 isotopologues with a permanent dipole, i.e. CO_2 molecules with the $C_{\infty v}$ point group.

The energy level of rotational states can be approximated with:

$$E_{\text{rot}} = \frac{hJ(J+1)}{8\pi^2 c\Sigma m_i r_i^2} \tag{7.4}$$

where h, c, m_i, and r_i are Planck's constant, the speed of light, the mass, and distance from the center of mass of particle i. The resulting rotational energy is quantized and increases quadratically with J. The energy difference between two levels, which is observed in absorption experiments, can be calculated by:

$$\begin{aligned} \Delta E &= \Delta E_{\text{final}} - \Delta E_{\text{initial}} \\ \Delta E &\propto (J+\Delta J)\cdot(J+\Delta J+1) - J\cdot(J+1) \end{aligned} \tag{7.5}$$

Pure rotational Raman transitions yield S-branches (ΔJ = 2) and O-branches (ΔJ = -2), which yield equidistant lines with 8B difference. For pure rotational infrared transitions, the energy difference is 2(J+1) for R-branches (ΔJ = +1) or -2J for P-branches (ΔJ = -1). The resulting rotational spectrum yields equidistant lines with 4B increments. While pure rotational infrared transitions are symmetry forbidden for CO_2, rotational excitation is allowed in combination with vibrational excitation. Equidistant rotational lines are observed for rotation vibration (rovibration) excitation. Before we go into rovibrations, we shall first introduce pure vibrations (also called normal modes or fundamentals).

Vibrations

Molecular vibrations are described reasonably well by the harmonic oscillator model: atoms within the molecule are masses attached to one another through springs. Bonded atoms are held together by strong springs. Unbonded atoms are connected through weaker springs to relax the molecule back to the overall molecular shape. Under the assumption that the amplitude of the vibration is infinitesimal, the energy level of the harmonic oscillator is described by:

$$E_{vib} = h\nu_i \left(\mathrm{v}_i + \frac{1}{2}\right) \tag{7.6}$$

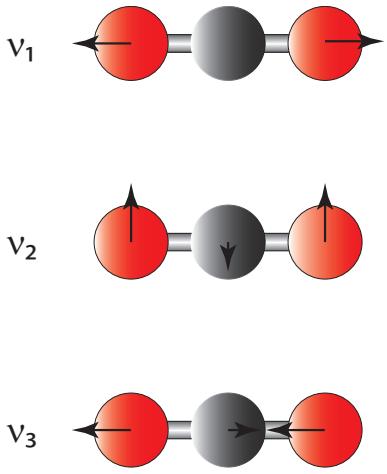

Figure 7.2: The ν_1 symmetric stretch, degenerate ν_2 bend, and ν_3 asymmetric stretch vibrations.

where ν_i and v_i are the frequency and vibrational quantum number of normal mode (or fundamental vibration) i. The energy level of the harmonic oscillator increases linearly with v_i.

CO_2 has 4 vibrational degrees of freedom: ν_1, double degenerate ν_2, and ν_3. These three normal modes are shown in figure 7.2. Ground state CO_2 has Σ_g^+ character. The symmetry of the molecule may change upon excitation of one or more quanta of vibration, in which case the transition is infrared active.

ν_1 is the symmetric stretch vibration with Σ_g^+ character. In this fundamental, the oxygen atoms move in phase towards and away from the carbon atom in the center of mass. There is no change in symmetry and therefore no change in dipole moment. This mode is only Raman active. The transition occurs at approximately 1388 cm^{-1}.

ν_2 is the double degenerate bend vibration with Π_u character. In this mode, vibrationally excited CO_2 bends so that the OCO bond angle is not 180° anymore. The oxygen atoms move orthogonal to the intermolecular

axis, while the carbon atom moves in the opposite direction to conserve the center of mass. Excitation of the bend vibration results in a superposition of the two degenerate modes and generates vibrational angular momentum ($\Delta\ell = \pm 1$). This degeneracy and angular momentum gives rise to rotation around the bond axis on excitation of the bend vibration. There is a change in symmetry and dipole moment on excitation of the bend vibration. Consequently, this mode is infrared active. The transition occurs at approximately 667 cm^{-1}.

ν_3 is the asymmetric stretch vibration with Σ_u^+ character. The oxygen atoms move out of phase along the bond axis. Here, the carbon atom moves along the intermolecular axis to preserve the center of mass. The change in dipole moment means that this mode is infrared active. The transition occurs at approximately 2350 cm^{-1}.

Rovibrational transitions

The selection rules for exciting a vibration in a CO_2 molecule depend on the symmetry and vibrational angular momentum ℓ of the initial and final state. The selection rules are also consequential for the spacing between the rotational lines; they determine whether odd rotational levels exist or not. The following selection rules apply for $D_{\infty h}$ molecules:

1. $\Delta\ell = 0$, $\Delta J = \pm 1$ (i.e. $\Sigma - \Sigma$ transitions)
2. $\Delta\ell = \pm 1$, $\Delta J = 0$ or ± 1 (e.g. $\Pi - \Sigma$, $\Delta - \Pi$ transitions)
3. $\Delta\ell = 0$ and $\ell \neq 0$, $\Delta J = 0$ or ± 1 (e.g. $\Pi - \Pi$ transitions)

The first selection rule is exemplified by the ν_3 rovibrational transition in CO_2; i.e. the transition of interest for this work. Excitation of this rovibration results in a P-, and R-branch, but no Q-branch ($\Delta J = 0$). As ℓ remains 0 and $\Delta J = \pm 1$, excitation of the ν_3 vibration changes the vibrational and rotational quantum numbers v and J by 1. The rotational lines show a 4B separation.

The second selection rule constitutes a change in ℓ, which occurs for the ν_2 bend vibration in CO_2. Here, ΔJ may be 0 or ± 1. Consequently, excitation of the ν_2 rovibration exhibits a P-, Q-, and R-branch. Quantum numbers v and ℓ are changed with 1, while J may remain the same or change by 1. These rotational lines also show a 4B separation.

ℓ does not change for the final selection rule, but the initial state is already vibrationally excited (hot band transitions) with vibrational angular momentum. This is the case for CO_2 on excitation of the ν_3 vibration with one or more quanta of ν_2 in the initial state. Excitation may occur from both odd and even initial rotational states, due to P-, Q-, and R-branches being available for bend vibrations. The rotational line spacing for these rovibrational transition is therefore 2B.

Anharmonicity of rovibrations

We started off on the premise that normal modes have different symmetry and that these vibrations can be described by the harmonic oscillator model. The harmonic oscillator model assumes that vibrations can be disentangled into normal vibrations. However, the harmonic oscillator model fails when mixing and coupling occurs between the different normal modes under certain conditions. The three main sources for deviations from the harmonic oscillator model for linear molecules are: ℓ-type doubling, Fermi resonance, and Coriolis coupling.

ℓ-type doubling occurs for overtones of the bend vibration of CO_2. As mentioned previously, ν_2 excitation changes the vibrational angular momentum ℓ. ℓ has two possible directions when $\Delta\ell = \pm 1$. $1\nu_2$ has $\ell = +1$ or ℓ = -1, which are identical in energy. However, overtones of the ν_2 are degenerate and cause ℓ-type doubling; e.g. for $2\nu_2$ the vibrational levels split for $\ell = 0$ and $\ell = \pm 2$.

An additional anharmonicity occurs for overtones of the bend vibration with $\ell = 0$. $2\nu_2$ with $\ell = 0$ has the same symmetry (Σ_g^+) and very similar energy as the ν_1 symmetric stretch vibration. Consequently, the $2\nu_2$ overtone

with $\ell = 0$ and ν_1 fundamental are in Fermi resonance. These vibrational states mix and are indistinguishable. In addition, the energy levels that are in Fermi resonance are perturbed; i.e. the separation between the energy levels is much larger than expected. Two peaks are observed in Raman for the ν_1 vibration due to the Fermi resonance with $2\nu_2$. While we would expect $2\nu_2$ to be roughly twice the ν_2 normal mode, both Raman peaks are separated significantly from the expected $2{\cdot}667$ cm^{-1} for the $2\nu_2$ vibration due to the perturbation.

The previous anharmonicities deal with the symmetric stretch and bend vibrations. The Coriolis effect affects the asymmetric stretch and bend vibrations. During a pure normal mode vibration without rotation, the atoms move linearly as shown in figure 7.2. Vibrational and rotational motion induces vibrational anharmonicity due to the Coriolis effect. This concept is visualized in figure 7.3. Consider the normal vibrations shown in figure 7.3a. The linear motion of the atoms relative to the center of mass during vibration is indicated in black. Counter-clockwise rotation of the molecule is shown with blue arrows. The linear motion due to vibration in the rotating frame gives rise to a fictitious Coriolis force perpendicular and proportional to the velocity of the vibration. These Coriolis forces are shown in figure 7.3a as green arrows. The Coriolis force direction for the various normal modes shows that some normal modes couple to one another in the rotating frame. This is shown in figure 7.3b with white arrows tracing the motion of the atoms. The ν_1 vibration itself does not exhibit Coriolis coupling to other normal modes; it couples to rotation. However, the ν_2 and ν_3 vibrations do couple to one another and mixing of the two occurs. The ν_2 bend vibration of rotating CO_2 also exhibits some ν_3 asymmetric stretch vibration with the frequency of ν_2. Similarly, ν_3 induces a ν_2 bend vibration with the frequency of the ν_3 vibration.

State preparation of CO_2 in the supersonic molecular beam

Now that we have immersed ourselves in the spectroscopy of CO_2, we focus on experimentally preparing a CO_2 supersonic molecular beam in a specific

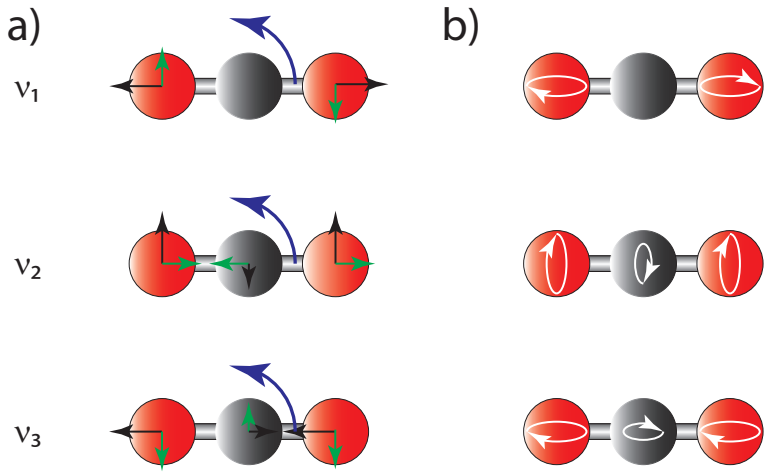

Figure 7.3: The Coriolis effect for the ν_1 symmetric stretch, ν_2 bend, and ν_3 asymmetric stretch vibrations. a) Molecular rotation, motion of the atoms, and the Coriolis force is indicated with blue, black, and green arrows respectively. b) Motion of the atoms in the rotating frame is shown with the white arrows in the right set of figures.

rovibrational state. The UHV apparatus is described in detail in chapter 2. For excitation, infrared (IR) radiation from a continuous wave (CW) light source is crossed with the CW supersonic molecular beam. The excitation scheme is based on that developed by Bruce Yoder[136] from the group of Rainer Beck. Excitation of CO_2 occurs if IR radiation is resonant with the optical transition: the ν_3 asymmetric stretch vibration at approximately 2350 cm^{-1}.

The optical setup is shown in figure 7.4. The setup is built up on a laser table and enclosed in an aluminum box that is purged with dry nitrogen. Approximately 300 mW of tunable IR radiation is generated by a commercial Optical Parametric Oscillator(OPO, Lockheed Martin Aculight, Argos Model 2400, SF-15, Module D). Of the 300 mW, 50% is sent to the UHV chamber for state-preparation. The other 50% is used for characterization and stabilization. A CaF_2 window samples a small amount (5%) for the wavemeter (λ). The remainder is retroreflected through a CO_2 gas cell for Lamb dip spectroscopy for actively stabilizing the OPO.

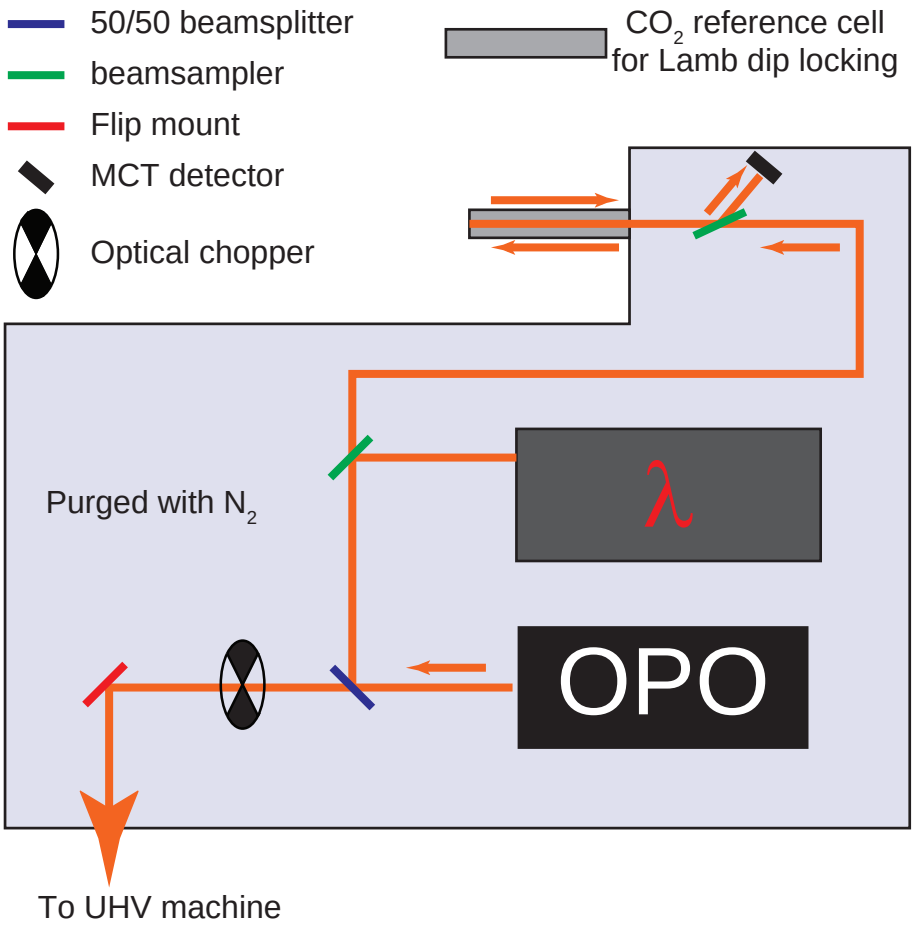

Figure 7.4: Optical setup used to characterize and actively stabilize the OPO.

We prepare CO_2 in a specific rovibrational state using single mode CW tunable infrared radiation. The light source of choice is a commercial Optical Parametric Oscillator. An OPO converts high energy photons into two lower energy photons. Total energy is conserved:

$$E_{pump} = E_{signal} + E_{idler} \tag{7.7}$$

For historical reasons, the two low energy photons produced are called signal and idler, of which the latter is lowest in energy. Four different available OPO modules offer the Argos system a broad spectral range from 2.3 – 4.6 μm (4348 – 2147 cm^{-1}). Our D module gives access to: 3.9 – 4.6 μm. (2564 – 2147 cm^{-1})

The OPO module is pumped by a 15 W amplified (IPG Photonics) 1064 nm Yb-doped seed laser (NKT-photonics) that is part of the Argos system. The OPO module consists of two parts: a periodically-poled lithium niobate (PPLN) nonlinear crystal placed within a bowtie etalon as optical resonator. Periodic poling of the nonlinear crystal determines the E_{signal}:E_{idler} ratio. Upon exceeding a threshold power, idler and signal photons are generated. The signal beam is resonant within the etalon and builds up power within the resonator cavity. The photon conversion process is thereby amplified, increasing the idler output power.

The ν_3 R(0) transition for CO_2 occurs at an idler wavelength of approximately 4255 nm. From equation 7.7 and a 1064 nm pump wavelength, we calculate a signal wavelength of 1419 nm. The resulting signal and idler wavelengths present the first problem. The two most abundant infrared absorbers in air – H_2O and CO_2 – absorb signal and idler power respectively. Idler absorption lowers the available power for CO_2 excitation and OPO stabilization. Signal absorption by H_2O presents a bigger challenge: the signal power within the cavity can drop below the power threshold and stop the OPO from oscillating altogether. Consequently, the OPO becomes unstable when the signal is absorbed by water. Absorption by these air constituents requires purging the entire optical setup with dry nitrogen.

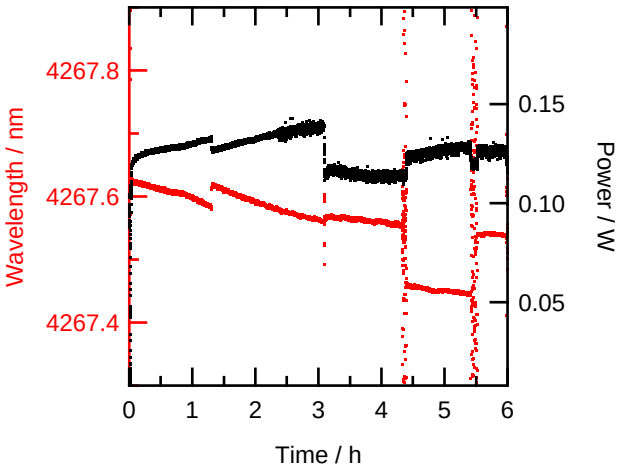

Figure 7.5: Idler wavelength (red, left axis) and power (black, right axis) as a function of time, exemplifying drift of the OPO.

The second problem to overcome is common for state-selective molecular beam experiments using a tunable light source. The linewidth of the light source and the natural linewidth of CO_2 in the supersonic molecular beam are extremely narrow. State-resolved experiments require reliable CO_2 excitation, i.e. the wavelength of the OPO preferably matches the transition for hours. Figure 7.5 shows the idler wavelength and power as a function of time, as measured using the wavemeter (Bristol, 621B-IR) and calibrated power meter (Thorlabs, PM100D). Three notable features are observed. First, the idler wavelength drifts substantially over time. Second, discrete jumps are observed, showing mode hops. Third, the wavemeter reading goes off scale at approximately 4 hours due to a drop in power. The overall wavelength drift of the OPO shows that active stabilization is required for long term experiments. Mode hops generally disappear or lower in frequency as the OPO stabilizes. Active stabilization cannot completely prevent these.

The idler wavelength can be tuned in three ways. Rough tuning uses the varying periodic poling across the crystal. By vertically translating the

PPLN crystal, the periodic poling experienced by the pump laser changes. Alternatively, the crystal temperature can be changed to the same effect. However, temperature is not recommended for active tuning. Intermediate tuning alters the signal wavelength resonant in the cavity by changing the etalon angle. The idler wavelength changes accordingly. Fine tuning alters the 1064 nm pump wavelength. The pump, idler and signal wavelengths are blue-shifted by straining the seed laser optical fiber with piezo tuning(0 — 200 V).

Figure 7.6 shows calculated spectral line intensities from HITRAN[137] for exciting the ν_3 vibration at gas temperatures of 298 K and 5 K. For room temperature CO_2, the P- and R-branches are observed. The Q-branch is absent, as explained by the selection rules. In addition to the ν_3 fundamental, a weaker v = 1 (ν_2) $\rightarrow$ v = 2 (ν_2 + ν_3) hot band transition overlaps with the fundamental. It is blue shifted to higher wavenumbers compared to the fundamental. However, molecules prepared in the supersonic molecular beam are rotationally and translationally cold. The rotational state distribution in the molecular beam is illustrated by the calculated line intensities at 5 K shown in the top zoomed in panel. Rotationally cold CO_2 mostly resides in J = 0, 2, and 4. The bottom panel shows idler power as a function of wavenumber measured on two separate days by slowly (1.2 Vmin^{-1}) scanning the seed laser piezo. The power is measured after passing the idler through a 1.5 m long gas cell.

We point out two notable things. First, the spacing between the hot band transitions is approximately half that of the fundamental. For the hot band transition, the lower level has one quantum of ν_2 with symmetry. Second, there is a small offset ($\sim$ 0.02 cm^{-1}) between the HITRAN database and our measured absorption peaks. This offset likely results from a slight misalignment of the idler beam entering the wavemeter. However, the offset is not relevant for our experiments as the wavemeter is only used to find the optical transition. Active stabilization is necessary for stability, since the wavemeter does not have the required accuracy.

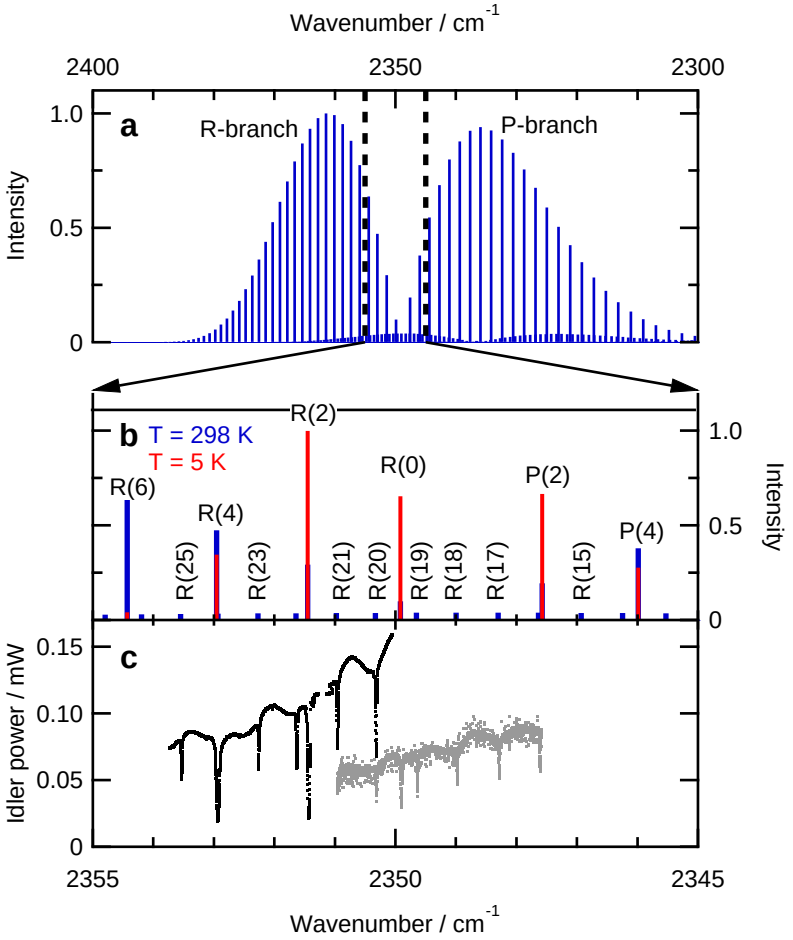

Figure 7.6: Transition line intensities for CO_2 at 298 K (blue) and 5 K (red) extracted from HITRAN.[137] The bottom panel shows two scans of the idler power measured on separate days. The power is measured after passing through a 1.5 m long gas cell containing 100 mbar (black) or 50 mbar (gray) of air.

In practice, setting the OPO to a specific wavelength is an iterative process of the following steps. The wavelength is set slightly red-shifted of the transition of interest using rough crystal tuning. Subsequently, the etalon angle is changed to maximize the idler output power. When a suitable amount of idler power is measured near the optical transition, the idler is tuned to the actual transition using piezo tuning.

To account for drift, we stabilize the OPO by locking onto the Lamb dip of the rovibrational transition.[136] We first explain the nature of the Lamb dip. Earlier in this chapter, we showed that absorption of radiation is quantized; i.e. a photon may be absorbed if the photon energy matches the energy difference between the initial and final state. In practice, absorption peaks in spectroscopy are broadened through various mechanisms, one of which is Doppler broadening. Doppler broadening occurs if absorbing molecules contain a velocity component along the propagation axis of the incident radiation. Those molecules then observe radiation with a frequency ν instead of ν_0:

$$\nu = \frac{c \pm v_i}{c}\nu_0 \tag{7.8}$$

where c and v_i are the speed of light and the velocity of absorbing particle i.

Figure 7.7 illustrates the concept of the Lamb dip. Panel a shows a Doppler broadened absorption profile. As high power monochromatic radiation pumps an optical transition slightly off resonance, a significant fraction of molecules with velocity v_i is excited. Panel b shows that the ground state population with $+v_i$ is reduced compared to panel a. The hole burnt in the population distribution for $-v_i$ is called a Bennett hole [138, 139], named after William Ralph Bennett Jr. The Bennett hole can be observed in absorption by crossing a probe beam of monochromatic radiation with the pump. A second Bennett hole is burnt in the population distribution when retroreflecting the pump beam through the gas cell in panel c. Finally, as the pump beam is tuned on-resonance with the transition in panel d, the forward and reflected beam probe the same subset of molecules: molecules

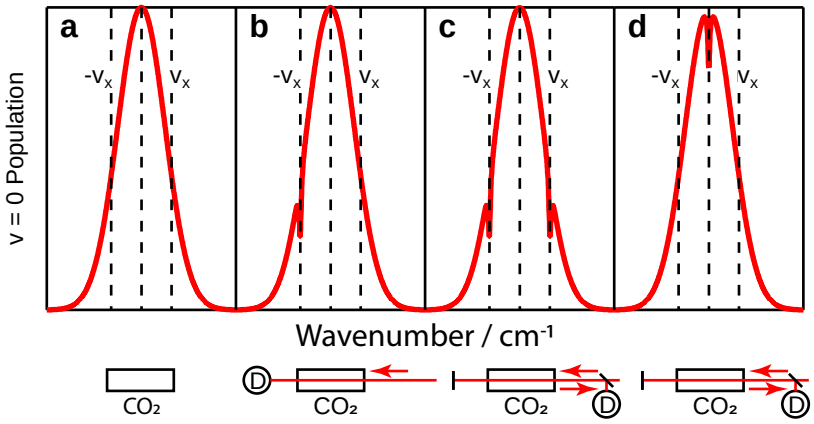

Figure 7.7: Illustration of Bennett holes and the resulting Lamb dip upon retroreflecting off and on resonance monochromatic radiation.

with $v_i = 0$ ms^{-1}. As the forward beam saturates the transition, fewer ground state molecules are available with $v_i = 0$ ms^{-1} for the retroreflecting probe beam. Consequently, a dip is observed in the absorbance spectrum. This Lamb dip[140] is named after Nobel laureate Willis Eugene Lamb Jr.

We use the Lamb dip to stabilize the OPO onto the optical transition, similar to Yoder et al.[136] Doppler broadened absorption peaks with and without Lamb dip are compared with a measured Lamb dip in figure 7.8. We measure the derivative of the absorption features using phase sensitive detection. The width of the Doppler broadened signal and its weak derivative signal near the transition limits its use for stabilization. However, the narrow Lamb dip feature and its strong derivative signal near the optical transition is ideal for active stabilization. The derivative provides the feedback with a sharp feature to lock onto.

We measure the reflected beam with a room temperature DC-coupled MCT detector (PDAVJ8, Thorlabs). Like Yoder et al., we use the Laselock (TEM-Messtechnik) for active stabilization. It combines all electronics required: a signal generator, the Lock-in amplifier, and a PID controller.

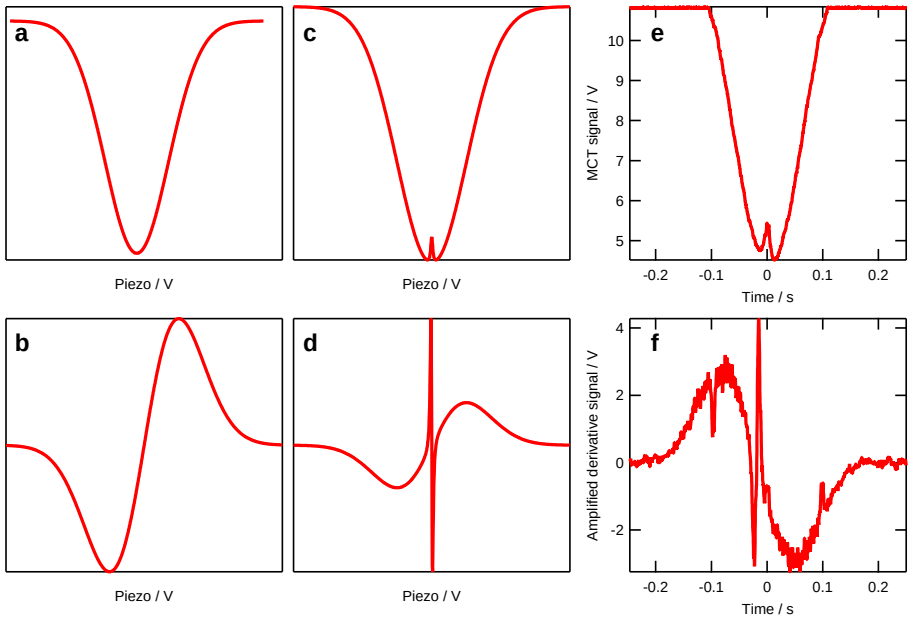

Figure 7.8: a) Simulated Doppler broadened absorption peak with b) its derivative signal. c) Simulated Doppler broadened absorption peak with a Lamb dip and d) its derivative signal. e) Measured Doppler broadened absorption peak with a Lamb dip and f) its derivative signal.

The signal generator applies a 4.8 mV (0.02%), 4 kHz dither to the seed laser piezo, resulting in a 0.17 pm (2.8 MHz) wavelength dither. The 4 kHz signal is sent to the lock-in amplifier as its reference input. The signal generator can superimpose a linearly sweep onto the dither to scan over an absorption line. In this way, the spectrum and its derivative in figure 7.8e and f are measured. The offset of the scan is set such that the absorption peak is centered. After observing a suitable Lamb dip, the scan generator is switched off and the PID regulator is switched on. The Laselock regulates the piezo so that the derivative of the Lamb dip is 0 V. Figure 7.9 illustrates the wavemeter reading while the idler is actively stabilized to the Lamb dip in this manner. In contrast to the instability and drift observed in figure 7.5, the wavelength is stable for over 30 hours, after which a mode hop breaks the stabilization. During stabilization, there is some drift in the measured wavelength. We attribute this to pressure and/or temperature

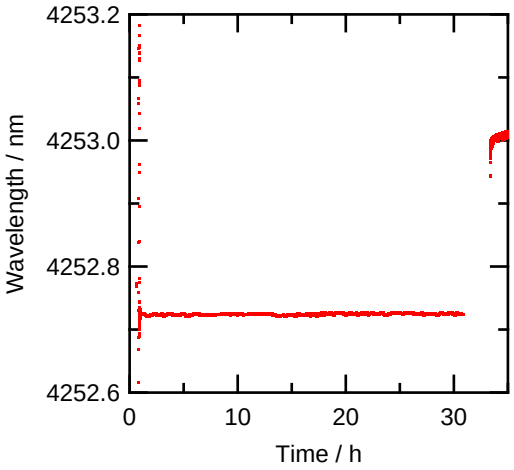

Figure 7.9: Idler stability during active stabilization of the R(4) transition.

fluctuations in the purge box influencing the wavemeter.

With the OPO stabilized to the vibrational transition, we may cross the idler with the supersonic molecular beam containing CO_2. The idler beam sent to the main chamber is periscoped up to the supersonic molecular beam. Two protected silver mirrors aid in steering the idler through the molecular beam at 90°. Normally, the transition is saturated if 50% of molecules are pumped to an excited state. However, by using Rapid Adiabatic Passage (RAP), population inversion can be achieved.[141] In RAP, defocusing of monochromatic radiation causes absorbing molecules to experience a frequency sweep due to curved wavefronts. To this end, we use a CaF_2 cylindrical lens (f = 200 mm, Thorlabs) to defocus the idler.[136, 141]

Finally, we require a method of detecting excited CO_2 molecules in the molecular beam. We use pyroelectric detection (PED) (406M39, Eltec Instruments), similar to that used by the groups of Art Utz and Rainer Beck.[136, 142] The PED works through the pyroelectric effect. A change in temperature polarizes the detector material, inducing a voltage over the detector element. As the temperature reaches steady state, the voltage

across the detector element is negated by current leaking from one side to another. Consequently, these detectors are AC-coupled and require a modulated signal.

First, we align the PED to the supersonic molecular beam. We use a diode laser to align the single crystal surface to the molecular beam. By retracting the molecular beam nozzle, the diode laser follows the same path through the skimmers as the molecular beam. The single crystal surface is aligned to the molecular beam by reflecting the diode laser back onto the sliding valve orifice. Here, we use this diode laser to align the PED as well, as the absolute signal from the diode laser is much larger than that of the molecular beam.

Figure 7.10 shows an overview of the UHV machine (Lionfish) in the top panel. It shows the modulated diode laser passing through the various skimmers before striking the PED. The PED is on a swivel so that it can rotated in and out of the molecular beam. The color of the PED traces shown in this and following figures in this chapter use modulation from the matching colored annotation. The bottom panel shows the raw PED data in red. We chop the laser with 11 Hz using the optical chopper (MC2000, Thorlabs). The optical chopper has a built in photodiode as reference output, shown in black. Note that there is a phase difference between the PED results and the reference output because the diode laser laser does not pass the chopper blade at the photodiode. The resulting PED signal is a 11 Hz triangular wave with an amplitude of approximately 68 mV. Modulated signals can be extracted with high signal-to-noise ratio with lock-in amplification. Using the lock-in amplifier, we extract the amplitude of the PED signal.

During beam experiments, we can modulate the molecular beam using the first beam flag, second beam flag, or the mechanical chopper. The mechanical chopper has two different slot sizes. This restricts its application for lock-in amplification, because the lock-in amplifier cannot extract the reference frequency. Meanwhile, the two beam flags can only modulate the

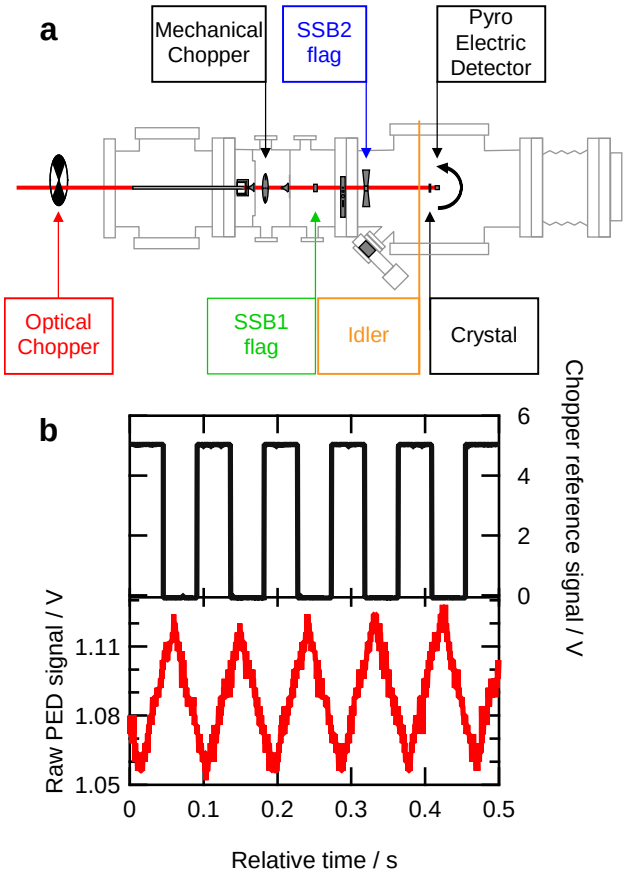

Figure 7.10: a) Schematic overview of the UHV machine, indicating the position of: the pyroelectric detector (PED), crystal, two beam flags, mechanical chopper, optical chopper, idler beam crossing the CO_2 beam during excitation. b) The PED transient is measured by modulating the diode laser with the optical chopper at 11 Hz.

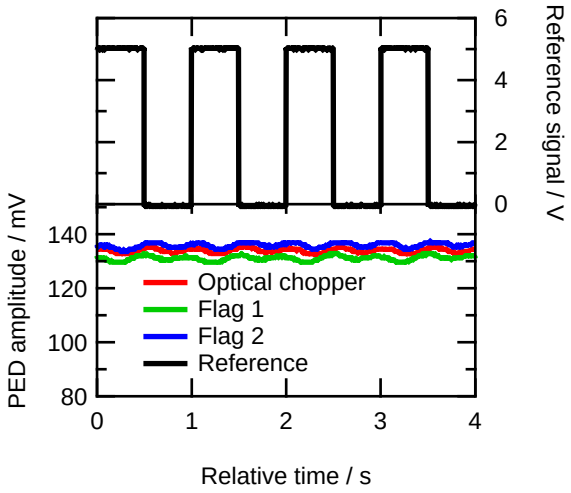

Figure 7.11: Amplitude of PED transients, as measured with the lock-in amplifier. The diode laser is modulated at 1 Hz using the optical chopper (red), first beam flag (green), or second beam flag (blue).

molecular beam with approximately 1 Hz. Figure 7.11 compares the signal amplitude when modulating the diode laser with the optical chopper, first flag, or second flag at 1.0 Hz. Overall, the amplitudes for the optical chopper and second beam flag are relatively similar. The first flag amplitude is slightly lower as a result of its gating function. It is a spring-loaded solenoid valve that opens faster than it closes, resulting in a slightly lower amplitude. The difference is minimal though.

With the PED working properly with the three methods of modulation, we can impinge a pure CO_2 beam expanded from a room temperature nozzle onto the detector. Both methods of modulation worked properly for the diode laser. Upon measuring the CO_2 beam, flag 2 modulation exhibited a significant amount of crosstalk (3 mV). While this was resolved by shielding the PED cables, results presented here were measured with flag 1 modulation without shielding. Figure 7.12 presents the PED amplitude measured with the lock-in amplifier. Flag 2 is either continuously open (green) matching flag 1 modulation or continuously closed (blue). Flag

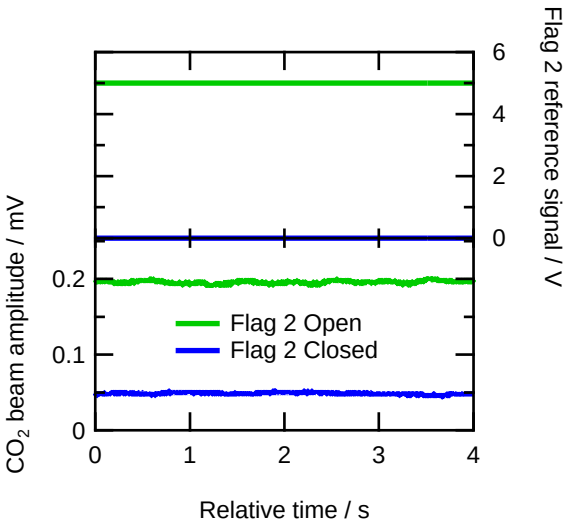

Figure 7.12: PED amplitude measured with the lock-in amplifier. The CO_2 molecular is modulated at 1 Hz using the first beam flag. Flag 2 is either continuously open (green) or continuously closed (blue).

2 being closed is a measure for crosstalk and CO_2 molecules striking the detector after scattering off flag 2. When flag 2 is open, the only difference is that CO_2 molecules can directly impinge onto the detector. We observe a 150 µV amplitude as a result, showing CO_2 molecules impinging the detector with 1.0 Hz.

Finally, we can move on to attempt detecting vibrationally excited CO_2 molecules in the supersonic molecular beam. Ordinarily, the best way to do this is by modulating the idler before it crosses the CO_2 beam and using lock-in amplification. For us, this presented a problem because we observe photons scattering off the CaF_2 windows. Instead, we take a similar approach as we did for detecting the CO_2 beam. We now compare the PED amplitude of actively stabilized idler radiation with off-resonance idler radiation. We emphasize that the idler is continuously on, while the lock-in amplifier detects only modulating signals. By modulating the CO_2 beam with 1 Hz, we either increase the internal energy of the CO_2 beam when the idler is resonant, or the internal energy remains the same. Figure 7.13 presents

the results. Figure 7.10a schematically shows where the idler crosses the CO_2 beam. Simultaneously with the PED amplitude, idler power is measured with the calibrated power meter after exiting the UHV. Two observations points towards CO_2 excitation in the molecular beam. First, the average PED amplitude for actively stabilized idler (189.6±0.10 μV) is higher than for off-resonance idler (186.2±0.10 μV). Second, idler power is slightly lower when it is resonant with CO_2 (26.5 ± 0.5 mW) than when the idler is tuned off-resonance (27.7 ± 0.4 mW), suggesting absorption by the beam.

We now discuss these results and their implications. Figure 7.13 shows that when the idler is stabilized, we observe a larger PED amplitude and lower idler power than when the idler is off-resonance. This is a consequence of vibrationally excited CO_2 in the molecular beam. The next step in the experiment is to determine the fraction of excited CO_2 by varying the idler power using the attenuator (Altechna, Watt Pilot). However, the amplitude increase for excited CO_2 (3.4 μV) is rather small. By comparison, E_{kin} from the pure room temperature CO_2 beam gives approximately 50 times more signal. From time of flight, we measure that E_{kin} is approximately 80 meV, while the rovibrational transition is 291 meV. There is a large discrepancy between the energy difference and the measured result. There are three explanations why there may be very little signal. First, the idler may not be adequately locked to the rovibrational transition. Second, the power may be too low for sufficient vibrational excitation (or the angle of the idler with the molecular beam is not 90°). Third, CO_2 may not be transferring its vibrational energy to the PED as efficiently as CH_4 does in the experiments by the groups of Art Utz and Rainer Beck. The first explanation is difficult to confirm if the third explanation is also part of the problem. Ideally, we confirm a good lock by using the pyroelectric detector signal. The second explanation seems unlikely, as Miller [143] used approximately 10 mW to show vibrational excitation of an HF beam. Similarly, Juurlink et al.[142] measured vibrational excitation of a CH_4 beam using just 2 mW of power. The third explanation may actually be the most plausible. For a 0.35 eV CH_4 beam, Yoder et al.[136] measure

1.5 V from the PED, after 10 x amplification. By comparison, we observe only 0.1% of this for our pure CO_2 beam. It has less E_{kin} to deposit, but more molecules to do so.

New experiments can ascertain the validity of these explanations. The first explanation is difficult to test on its own. Extra time focused on achieving a tighter lock may prove in vain. The second explanation can be confirmed or disproven by measuring PED signal as a function of idler power. The third explanation can be tested by using a different molecule, preferably with a rovibrational transition in range of our OPO module, and comparing its absolute PED signal to that of CO_2. Methane or acetylene are viable options that may not require purging, thereby making it easier to setup the experiments. Without excitation, the former enables direct comparison to results from the groups of Utz and Beck. If CH_3D or CD_4 is available, the quality of the lock can be verified by respectively exciting the ν_1 or ν_3 vibration. The PED signal can then also be compared to those from Utz et al. and Beck et al. for different isotopes.

The alternative to methane, acetylene, is a linear molecule with point group $D_{\infty h}$, similar to CO_2. It is likely to be more reactive than CO_2, thereby possibly generating more signal at the PED. When using the C_2D_2 isotope, the OPO can access the ν_3 asymmetric stretch vibration for comparison to the CO_2 PED signal. This could potentially set up future experiments that look at state-resolved acetylene dissociation, ideally using RAIRS to identify adsorbed species. Comparison of vibrational efficacies for the two linear molecules – CO_2 and C_2D_2 – would be an interesting venture for understanding gas-surface dynamics of linear polyatomic molecules. CO_2 is rather stable with a Gibbs free energy of -394.4 kJ/mol, while the latter is somewhat unstable with +209.2 kJ/mol.[144] To what extent asymmetric stretch vibrational energy assists in dissociating the two molecules may prove insightful in understanding dissociation of linear polyatomic molecules at catalytic surfaces.

In conclusion, we presented the basics of CO_2 spectroscopy and the initial steps for state-resolved CO_2 dissociation. Vibrationally excited CO_2 was detected in the supersonic molecular beam. Quantifying the amount of excitation in the molecular beam requires more signal at the PED. However, it is unclear why the absolute PED signal is so low. Suggestions are made for future experiments to identify the cause. One suggestion for new experiments involves using acetylene, a different linear molecules, and to eventually compare state-resolved dissociation experiments for CO_2 and acetylene.

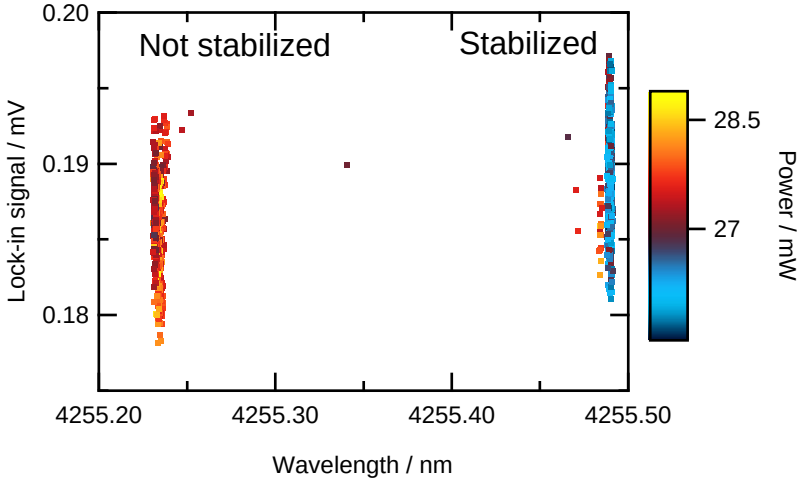

Figure 7.13: PED amplitude measured as a function of wavelength. The CO_2 molecular is modulated at 1.0 Hz using the first beam flag. Flag 2 is continuously open. The idler crosses the CO_2 molecular beam continuously, but is either frequency stabilized onto the R(0) transition or the stabilization is switched off so that the idler is off resonance.